ICAS 2020 SHANGHAI

32nd Congress
of the International Council
of the Aeronautical Sciences
September 6-10, 2021
Pudong Shangri-La, Shanghai, China

DYNAMIC RESPONSE AND DAMAGE OF THE FAN BLADES DURING UAV INGESTION INTO AN AERO-ENGINE

Naidan Hou[1,2,3], Xianghao Meng[1,2,3], Jun Liu[1,2,3] & Yulong Li[2,3,4]

[1]School of Aeronautics, Northwestern Polytechnical Univ., No. 127, Youyi West Rd., Xi'an 710072, Shaanxi, China
[2]Joint International Research Laboratory of Impact Dynamics and its Engineering Applications, Northwestern Polytechnical University, Xi'an 710072, Shaanxi, China
[3] Shaanxi Key Laboratory of Impact Dynamics and Engineering Application, Xi'an, China
[4] School of Civil Aviation, Northwestern Polytechnical University, Suzhou, China

Abstract

Based on the potential risk of a drone striking on an aircraft, a numerical model is established on the finite element analysis software PAM-CRASH version 8.6 to simulate the collision between a small drone and full-scale fan blades of a typical turbofan engine. Parameter studies are performed on the impact orientation, location and kinetic energy, and all are proved to have different levels of effects on the fan's dynamic response. In order to investigate the different damage mechanics of hard and soft impact, a comparative study is also conducted between the bird and the Unmanned aerial vehicle (UAV) ingestion with the same impact energy. Results showed that the damage and failure of the fan blades induced by UAV collision is more intense than that by bird strike due to its features of local stress concentration and material failure. The research results provide a reference for the revision of the airworthiness standards for small drones and the exploration of the test research of UAV airborne collision.

Keywords: UAV collision, engine fan blade, bird strike, numerical simulation, airworthiness

1. Introduction

Unmanned aerial vehicles (UAVs) have been one of the most promising industries in the aviation field in recent years. With the drastically increasing number of UAVs flying in the open air, most of the time without formal permissions, the potential risk of UAV airborne collision has increased profoundly. Therefore, damage assessment of aircraft structures under UAV impact should be investigated.

The engine fan is one of the most vulnerable structures on an airplane when confronted with a foreign object impact. Although airworthiness regulations of bird ingestion into aero-engines have been implemented [1], there is no evidence to guarantee the survival of airplanes after a UAV collision due to its feature of high hardness and nonuniformly distributed mass. Song et al. [2] conducted a comparative study on a high-bypass-ratio turbofan engine impacted by the UAV or bird, and found that a UAV was more destructive than a bird with the same mass. The authors also changed the impact conditions to evaluate the damage of the fan blade and the casing caused by the UAV collision. The Federal Aviation Administration (FAA) has drafted relevant regulations on UAV control [3], and released a series of research reports on UAV impact in 2017, among which the fourth part [4] carried out numerical simulation and damage assessment on UAV-engine impact. Up to now, the research on engine damage caused by UAV impact still remains to be developed.

This research aims to provide an insight into the dynamic response of an engine fan assembly under UAV collision and evaluate the severity of the fan's damage after such events by means of numerical simulation.

2. Computational Model

2.1 Engine fan assembly

The numerical model of the single fan blade used in this paper is provided by an engine company [5].

DYNAMIC RESPONSE AND DAMAGE OF THE FAN BLADES DURING UAV INGESTION INTO AN AERO-ENGINE

It is a typical wide-chord fan blade of a turbofan engine with high bypass ratio. The comprehensive finite element model is established on the explicit analysis software PAM-CRASH version 8.6 and can be identified in Fig.1(a). The thickness of the airfoil is the largest at the center, which gradually decreases on both sides along the chordwise direction. The blade is composed of an external panel and an internal corrugated board, between which are fused by coincident nodes. The thickness of the external panel is the largest at the root (2mm) and the smallest at the tip (1mm) along the spanwise direction. The internal hollow structure is 0.5mm thick, with the number of corrugation ranging from 10 to 20. Each joint between the inner and outer structure is 2.5mm long.

Considering the stress wave propagation in the direction of blade thickness, the hexahedral solid element with reduced integration is chosen to discrete the fan blades. Based on the mesh convergency study in [6], 5mm with 5 elements through the thickness is proved to be a good balance between mesh sensitivity elimination and computational efficiency. Therefore, each blade is divided into 56,250 elements, including 46875 elements in the external panel and 9375 elements in the internal core board.

The fan assembly consists of 18 hollow blades and its inlet diameter is 1.95m. The numerical model is shown in Fig.1(b). In this study, the deformation of the hub is relatively small compared with the damage deformation of the blades, and hence is simplified to a shell of cylinder with rigid constraint.
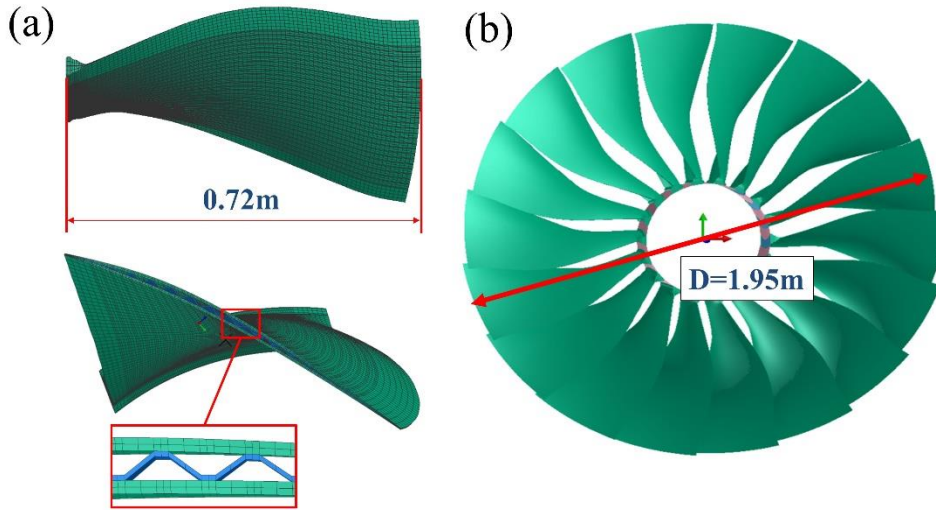

Figure 1 – Numerical model of (a)the single fan blade and (b) the fan assembly.

The mechanical behavior of the blade material Ti-6Al-4V (TC4) is defined by Johnson-Cook (JC) constitutive model integrating the strain rate effect, as is

$$\sigma = \left(a + b\varepsilon^n\right)\left(1 + c\ln\dot{\varepsilon}^*\right) \tag{1}$$

where $\dot{\varepsilon}^*$ is the dimensional plastic strain rate indicated as $\dot{\varepsilon}/\dot{\varepsilon}_0$ in which $\dot{\varepsilon}_0$ usually equals 1s⁻¹, and a, b, n, c are four undetermined parameters where a is the quasi-static yield stress, b is the initial hardening modulus, n is the work hardening coefficient, and c is the strain rate dependency coefficient. Failure behavior of the TC4 material is determined by JC failure model proposed by G.R. Johnson and W.H. Cook [7]. Combining the influences of the stress triaxiality and the strain rate on the failure strain of a material, this failure model could be expressed as:

$$\varepsilon_f = \left[D_1 + D_2 \exp\left(D_3\sigma^*\right)\right]\left(1 + D_4 \ln\dot{\varepsilon}^*\right) \tag{2}$$

where σ^* is stress triaxiality defined as $\sigma_m/\bar{\sigma}$ in which σ_m is the average of three principal stresses and $\bar{\sigma}$ is Von Mises equivalent stress, D_1, D_2, D_3 and D_4 are four material parameters to be determined. All the material parameters of TC4 used in this study are derived from Huang et al. [8] and listed in Table 1.

TABLE 1. Material parameters of TC4

Parameter	ρ(kg/m³)	E(GPa)	μ	a(MPa)	b(MPa)	n	c

Value	4440	114	0.33	891.5	630.1	0.547	0.034
Parameter	D_1	D_2	D_3	D_4			
Value	0.01546	1.349	-2.144	0.04323			

2.2 UAV

The drone model chosen for the engine ingestion is the Phantom 4, a typical small consumer quadcopter weighing 1.388kg from DJI Technology Co., Ltd., which is the world's leader in the civilian-drone manufacture. As is shown in Fig.2(a), The numerical model of the UAV consists of four main parts, which are the camera (0.259kg), the four motors (0.214kg), the lithium battery(0.468kg) and the chassis (0.281kg). Due to the complex inside structures of the original UAV, the numerical model of each part in this study is simplified to homogenous entities for the convenience of modeling and computation, while the major features are still retained.

Component	color	Mass/kg
camera		0.259
battery		0.468
motor		0.212
chassis		0.281
others		0.168
Total mass		1.388

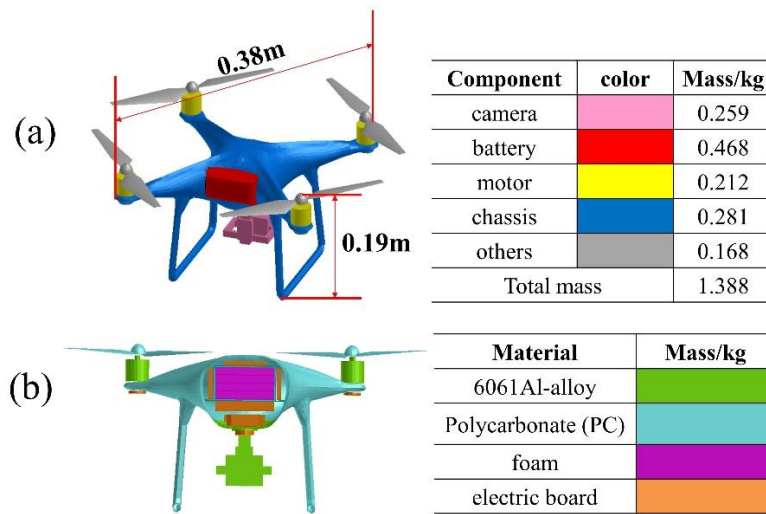| Material	Mass/kg
6061Al-alloy	
Polycarbonate (PC)	
foam	
electric board	

Figure 2 – (a)Components and their weights and (b) the material distribution of the UAV.

The finite element model of the drone has 8900 quadrilateral shell elements and 5044 hexahedral solid elements in total. Shell elements are applied to discrete thin-wall structures including the chassis, the fan blades and the battery shell, while solid elements are used for block components such as the battery, the camera and motors. An average mesh density of 5mm is proved to be sufficient in [9] and hence employed in this study.

The chassis is made of polycarbonate (PC) material and presented by the elastic-plastic model with ideal plasticity (Shell material type 105 in PAM-CRASH). The camera and motors are made of aluminum alloy and the JC constitutive model related to strain rate is selected (Solid material type 16 in PAM-CRASH). The lithium-ion battery is often treated as a crushable foam [10] and therefore a foam material model (Solid material type 24 in PAM-CRASH) is applied in this paper. The failure behavior of all the materials is determined by the equivalent failure strain ε_f, that is, the element will be deleted when the equivalent plastic strain of the element exceeds the failure strain ε_f of the material. All the material parameters are accessed from [9] and displayed in table 2. The material distribution of the whole UAV is mapped in Fig.2(b).

TABLE 2. Material parameters of UAV

Material	ρ(kg/m^3)	E(GPa)	μ	a(MPa)	b(MPa)	n	c	ε_f
6061-T6	2700	68.9	0.33	324	114	0.42	0.002	0.12
Material	ρ(kg/m^3)	E(GPa)	μ	Yield stress σ_y(MPa)			ε_f	
PC	1180	2.35	0.3	62			0.2	
Material	ρ(kg/m^3)	E_c(GPa)	E_t(GPa)	ε_f				
Li-battery	2150	0.63385	2.767	0.2				

2.3 Collision scenarios

3

A numerical model is established based on the PAM-CRASH explicit algorithm to analyze the collision between the small drone presented in Section 2.2 and full-scale fan blades of a typical turbofan engine elaborated in Section 2.1. In this study, the fan's rotating speed is set to 3,500rpm considering the typical working conditions of civil aircraft taking off at maximum thrust, and the impact speed of the UAV is set to 102m/s. The rotating speed is defined on a center of gravity (COG) node where the engine shaft is located. The velocity vector of the UAV is perpendicular to the rotating plane of the fan. This working condition acts as a baseline collision scenario, shown in Fig.3, and results are analyzed in Section 3.1.
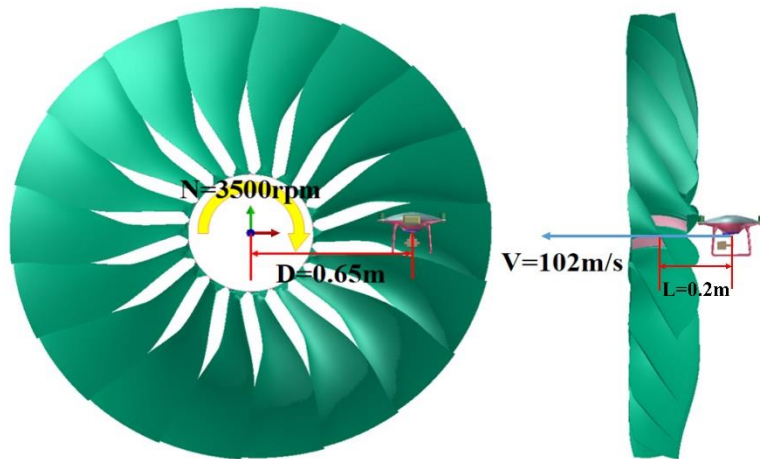
Figure 3 – Baseline collision scenario.

Parameter studies should be performed to figure out the impact factors that influence the deformation and damage of the fan blades under UAV collision. In this study, the effects of impact orientation (Section 3.2), impact location (Section 3.3) and impact energy (Section 3.4) are investigated and evaluated.

Impact orientation refers to the drone's attitude when striking the blades, including the yaw angle (Fig.4(a)) and pitch angle (Fig.4(b)). In real working conditions, the drone is ingested with a random attitude due to the air turbulence, and hence the critical attitude causing the worst consequence should be found. Typical values are predetermined based on the symmetrical features of the UAV's geometry profile.
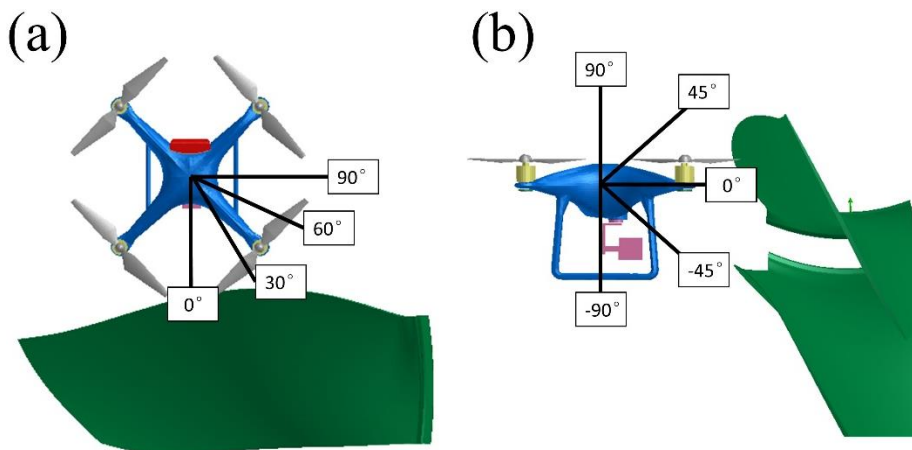

Figure 4 – Impact orientation including (a) the yaw angle and (b) the pitch angle.

Impact location refers to the relative position between the UAV and the blades, which incorporates the radial location (Fig.5(a)) and circular location (Fig.5(b)). Since the fan blade rotates with high speeds during impact, the linear velocity increases gradually from the root to the tip of the blade. Therefore, the radial location of the projectile determines the relative impact velocity of UAV and the blades, which may cause different consequences. On the other hand, the circumferential position of the impact point relative to the fan is also uncertain when the foreign object is ingested into the engine.

For a bird impact, the effect of circular impact location on the bird slices and the fan's damage can be ignored because the bird surrogate usually features a regular geometric shape. For a non-uniform UAV, however, the circular position determines the cutting direction of the blade against the UAV, leading to the fan's damage to be direction dependent.
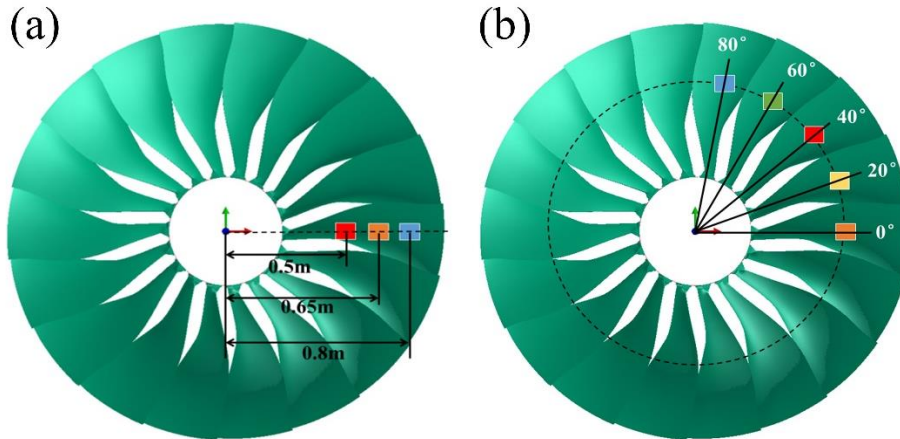

Figure 5 – Impact location including (a) the radial location and (b) the circular location.

Impact energy refers to the relative kinetic energy between the drone and the fan blades which is controlled by the drone's weight, the drone's linear velocity and the fan's rotating speed. The drone's weight is related to its inherent properties and hence keeps constant in this study. On account of the baseline condition, the drone's velocity is adjusted for other two scenarios, which are take-off (80m/s) and below 10000ft flight (129m/s). The fan's rotating speed varies from 3000rpm to 4000rpm according to the properties of the aeroengine provided by the engine company.

2.4 Bird model

In order to further explore the difference between hard and soft impact, a comparative study between UAV and bird ingestion into the aero-engine will be conducted in Section 3.5. A bird model with the same mass as the UAV is established and presented in Fig.6. Based on the previous studies [11][12], a hemisphere-ended cylinder with the length-to-diameter ratio of 2:1 is recommended to be the geometry of a substitutive bird. The length of the bird model (l) in this study can be calculated from the following equation

$$l = \sqrt[3]{\frac{96m}{5\rho\pi}}$$
(3)

in which the density of the bird (ρ) is 950 kg/m^3 derived from Lavoie et al [13]. If the bird mass m= 1.388kg is substituted, its length is determined to be 0.207m.
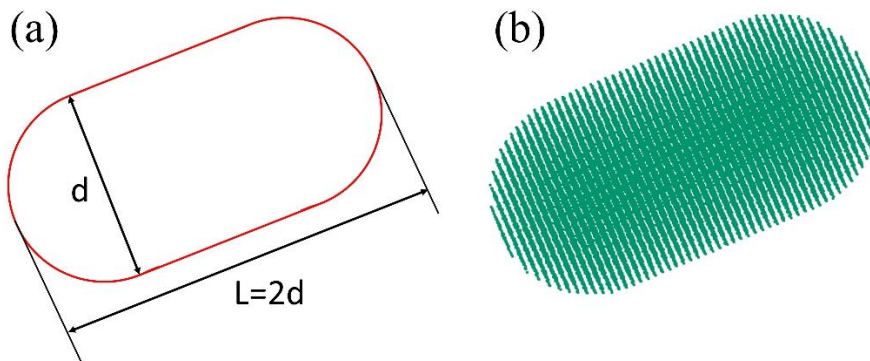

Figure 6 – Bird surrogate (a) the geometry and (b) SPH model.

Compared to traditional Lagrange mesh, a meshless method of Smoothed particle hydrodynamics (SPH) [14] can better simulate the fluid behavior of large deformation, crushing and splashing during the process of bird collision [15], and hence is applied to mesh the bird in this paper. The total number

of SPH particles for the bird is 23368.

The Murnaghan Equation of state (EOS) is adopted to describe the mechanical behavior of the bird as follows,

$$p = p_0 + B\left[\left(\rho/\rho_0\right)^{\gamma} - 1\right] \tag{4}$$

where p_0 is the initial pressure, p is the current pressure, ρ_0 and ρ are the initial density and current density, B is the bulk modulus, and γ is the amplification factor. In the numerical simulation of this paper, the parameters B =0.128 Gpa and γ =7.98 were determined by [16].

3. Results and discussion

3.1 A baseline scenario of UAV-fan collision

Fig.7(a) demonstrates the UAV-fan impact actions at different moments under the baseline scenario defined in Fig.3. According to Fig.7(a), the drone came into contact with four blades during the whole impact event of about 4ms. It is noted that the fan blades that had not been impacted are hidden for the convenience of observation. The first contact occurs at t=0.8ms, when the leading edge of the first blade (named Blade 1) collides with a motor and cuts a drone's fan. At t=1.6ms, the second blade (Blade 2) starts slicing two arms of the drone and then impacts with another motor. When t=2.2ms, the third blade (Blade 3) slices the bottom bracket of the UAV and after 0.5ms cuts the other two arms. At t=3.5ms, the rest of the drone begins to strike with the fourth blade (Blade 4) and meanwhile the slipping on Blade 3 still continues. The whole collision event is terminated at 4.7ms when all the debris have flown through the engine fan. Fig.7(b) depicts the drone's partitions sliced by each blade from the top and lateral view, in which Blade 3 is impinged on the largest segment including the lithium battery, the camera, and the main part of the chassis. It is also proved in Fig.7(c) that the specific mass of the UAV fragment impacting on Blade 3 is far larger than that on other blades.
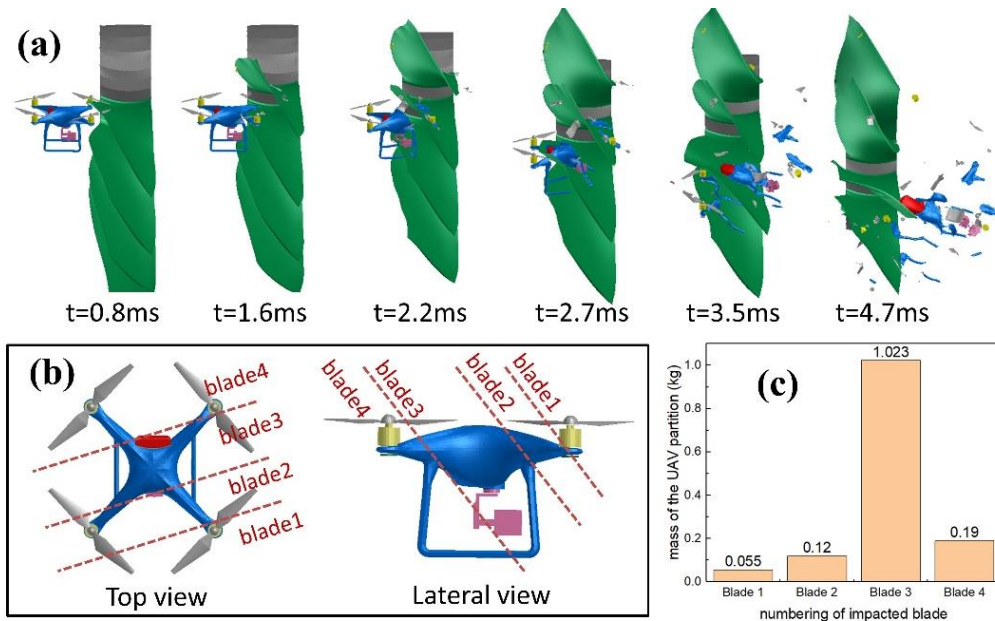

Figure 7 – Results of the baseline scenario (a) UAV-fan impact actions at different moments, (b) the drone's segments and (c) their mass sliced by each blade.

Fig.8(a) extracts the time history of contact force of Blade 3 as well as several typical states during the impact, in order to investigate the colliding mode between UAV and a single fan blade in detail. It can be found that the leading edge of Blade 3 first incises the bottom bracket of the drone, and then cut the rear two arms. The cutting process is finished about 1.5ms later. In the next moment, the residual UAV partition impinges with the concave surface of Blade 3, directly inducing the peak value of the contact force. Afterwards, the drone continues to slip along the direction of speed to the trailing edge of the blade with the contact force persisting declination, lasting about 2.5ms. Therefore, the collision process between UAV and a single blade can be divided into two typical stages, which are slicing and impacting.

The energy transmission of an engine fan subjected by a foreign object impact has been studied in

our previous paper [6], in which conclusions could also be proved in this study. If a foreign object (which is UAV in this study) impacts the rotating fan, the fan will lose its kinetic energy and transmit mainly to three sectors, as shown in Fig.8(b). The largest proportion is the projectile's kinetic energy, which accelerates the UAV after impact (accounting for 52.3%). The second is the fan's internal energy induced by the deformation and failure of fan blades (taking up 23.6%). The last is the projectile's internal energy for the drone's deformation and breakdown (taking up 13.3%). The specific percentages vary with different working conditions within reasonable errors, while the ranking remains the same. Fig.8(c) compares the increased energies of different components of the UAV, finding that the battery seems to be the most dangerous part that absorbs the largest quantity of kinetic energy while deforms little.
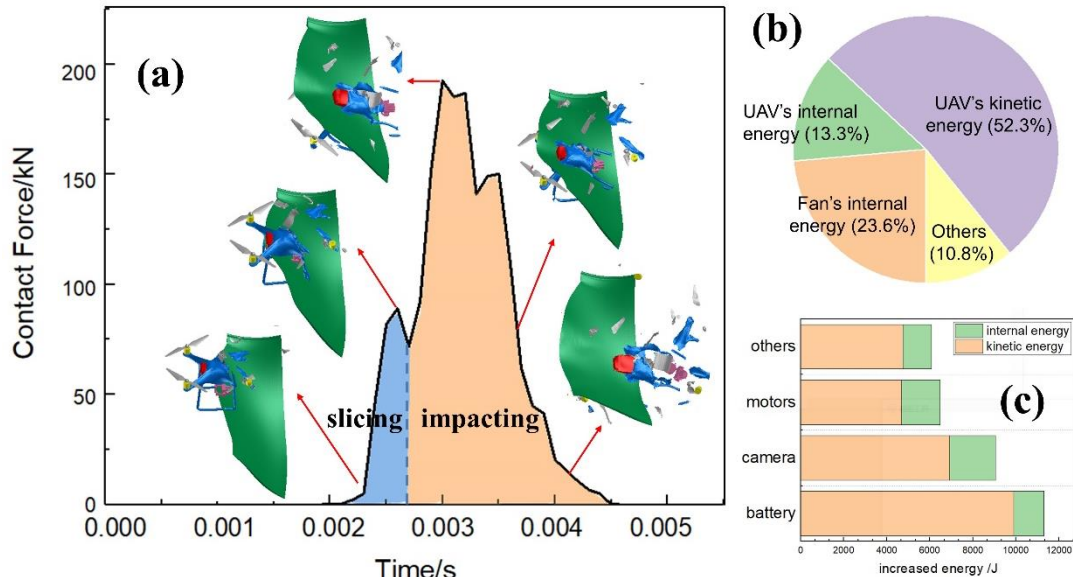

Figure 8 – (a) Typical impacting states and time history of contact force of a single blade, (b) energy transmission of the UAV-fan impact and (c) increased energies of different components of the UAV

3.2 Effect of impact orientation

In this section, the effect of the UAV's orientation (including yaw and pitch angles) on the fan's deformation is investigated. Based on the baseline scenario in Section 3.1, three different working conditions are determined by adjusting the drone's yaw angle from 0° to 30°, 60° and 90° (shown in Fig.4(a)), while other parameters remain unchanged. According to the results displayed in Fig.9(a), it is hard to observe the distinctions in the fan's plastic deformation. Therefore, the fan's internal energy and the maximum equivalent plastic strain are introduced to evaluate the fan's deformation quantitively, as shown in Fig.9(b). It can be concluded that the most severe collision seems to happen when the drone's yaw angle is 0°, while in fact the variation of the yaw angle has very limited influence on the fan's deformation.
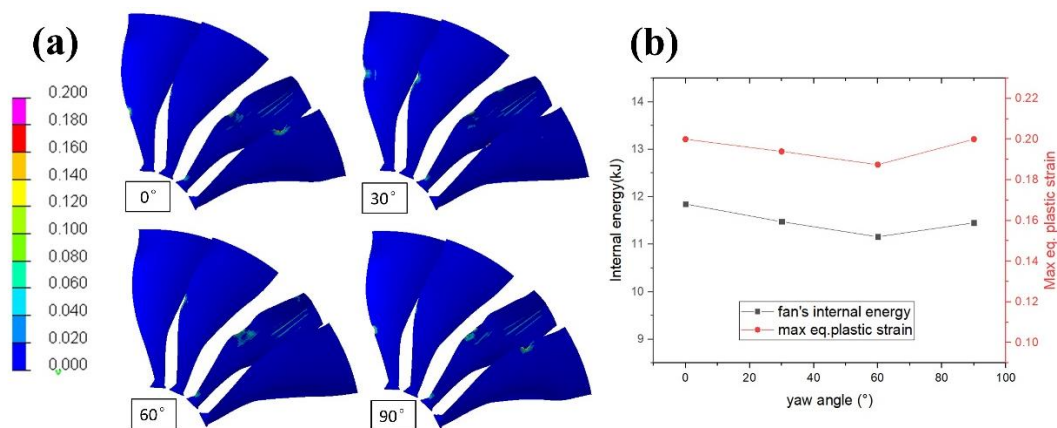

Figure 9 – (a) Contour plot of the equivalent plastic strain of the fan blades shortly after the UAV collision with different yaw angles, (b) changing curves of the fan's internal energy and the maximum equivalent plastic strain with the variation of the yaw angle

7

Now the pitch angle is the factor to be considered. As is depicted in Fig.4(b), five scenarios with different pitch angles of -90°, -45°, 0°, 45°, 90° are studied, in which other conditions keep the same with the baseline scenario. Fig.10(a) illustrates the contour plot of the equivalent plastic strain of the impacted blades. Results show that the UAV with the pitch angle of -90° or 45° induces higher level of fan's deformation than with the other angles. In order to quantify the effect, two indicators are determined for comparison, namely the fan's internal energy and the number of blades with material removal. The maximum equivalent plastic strain cannot be a reasonable index here because the material failure has already occurred in plenty of blades. According to Fig.10(b), both two indicators show a similar tendency when the pitch angle changes from -90° to 90°. Both the -90° and 45° scenarios result in three blades with material failure, while the fan's internal energy is larger for the 45° pitch angle. Hence, the pitch angle affects the fan's deformation a lot, and the most serious consequence occurs to the fan blades impacted by the drone with the pitch angle of 45°.
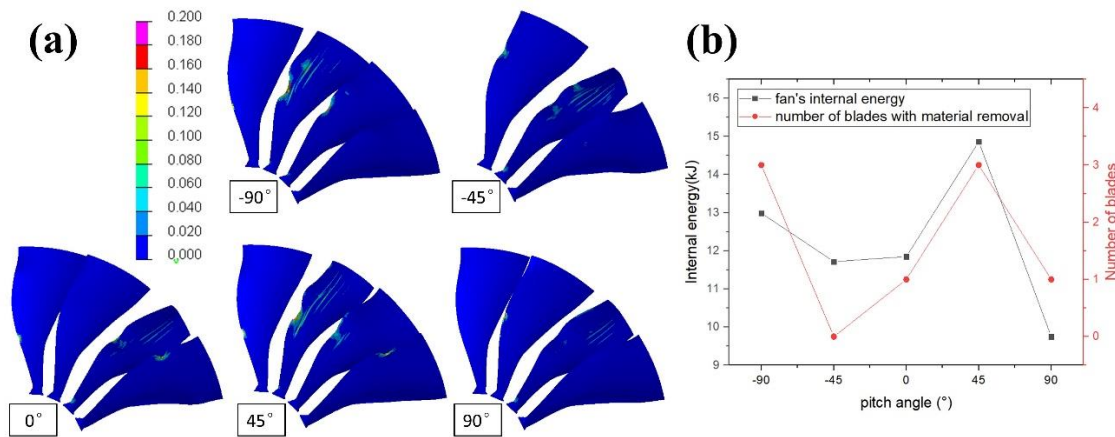

Figure 10 – (a) Contour plot of the equivalent plastic strain of the fan blades shortly after the UAV collision with different pitch angles, (b) changing curves of the fan's internal energy and the number of blades with material removal with the variation of the pitch angle

3.3 Effect of impact location

In this section, the effect of the UAV's impact location (including the radial and circular locations) on the fan's deformation is investigated. As is illustrated in Fig.5(a), taking the fan rotation axis as the origin, three impact positions were selected along the radial direction, namely 0.5m, 0.65m and 0.8m. It is clearly demonstrated in Fig.11(a) that the damage degree of fan blades gradually increases from the root to the tip. Especially in the 0.8m scenario, one of the blades severely bends and hence intersects with the adjacent blade. For the purpose of verifying the qualitative results above, two indicators are plotted and compared in Fig.11(b), including the fan's internal energy as well as the maximum Von-mises stress of the blade root. Additionally, the same element of the blade root is selected in each case for a fair comparison. Results show that both the indicators gradually increase with the drone impacting from root to tip, which is attributed to the increasing linear speed of the blades. Therefore, the radial impact position of UAV exerts a crucial effect on the deformation of the fan blades. The closer the drone is to the blade tip, the larger the impact velocity will be, thus causing a higher damage severity in the fan blades.
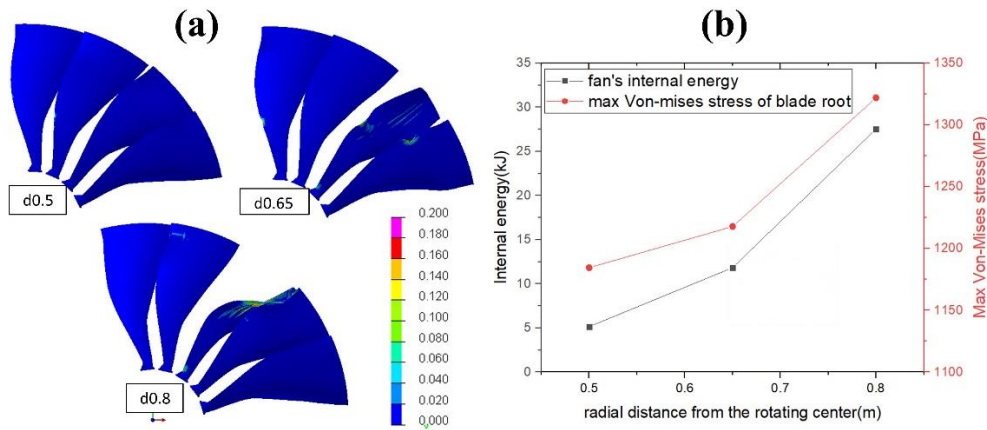
Figure 11 – (a) Contour plot of the equivalent plastic strain of the fan blades shortly after the UAV collision with different radial locations, (b) changing curves of the fan's internal energy and the maximum Von-mises stress of the blade root with the variation of the radial location.

The other parameter to be studied is the annular location. Since the angle between adjacent blades is 20°, each impact point is selected at an interval of 20° on the same circumference (r=0.65m), with a total of 5 impact points 0°, 20°, 40°, 60° and 80°, as shown in Fig.5(b). It can be observed in Fig.12(a) that the 0° and 80° scenarios provoke more significant response on the fan blades than the others, though the variation trend seems unclear. Therefore, the fan's internal energy and the maximum equivalent plastic strain are plotted in Fig.12(b) for detailed comparison. Results reveal distinctly that both the two indicators first descend with the circular location gradually increases, and then ascend after achieving the bottom at 40°. The 80° condition is slightly more severe than the 0° condition by comparing the fan's internal energy increased. To sum up, the severity of the fan's damage induced by UAV ingestion first falls then rises with the circular location changing from 0° to 80°, and the most dangerous consequence occurs when the drone interacts with the fan at 80° position.
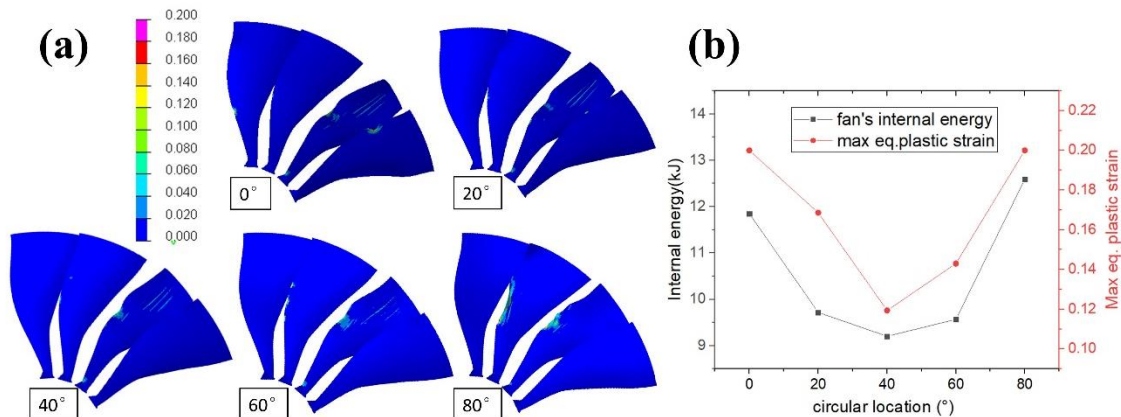

Figure 12 – (a) Contour plot of the equivalent plastic strain of the fan blades shortly after the UAV collision with different circular locations, (b) changing curves of the fan's internal energy and the maximum equivalent plastic strain with the variation of the circular location.

3.4 Effect of impact energy

In this section, the effect of the impact energy on the fan's deformation is investigated. Since the mass of the drone is constant in this study, the relative velocity of the drone and the fan is the factor to be discussed, including the drone's velocity (80m/s, 102m/s, 129m/s) and the fan's rotational speed (3000rpm, 3500rpm, 4000rpm). It is evidently illustrated in Fig.13(a)(b) that the drone poses a greater threat on the fan blades with the drone's velocity decreasing or the fan's rotational speed increasing. This phenomenon can also be proved in the results of the fan's internal energy plotted in Fig.13(c). It can be easily understood that the impact energy rises up as the fan rotates faster, leading to more plastic deformation and failure in the fan. Nevertheless, the more dangerous scenario apparently occurs when the drone's linear velocity decreases on the contrary. This seemingly abnormal result has been explained in our previous study [6], in which the velocity of the projectile contributes more on the impact duration than on the impact kinetic energy when interacted with a rotating fan. The

larger the drone's velocity is, the shorter the interaction lasts, thus resulting in less damage in fan blades. Briefly speaking, the fan's rotational speed is a dominant factor of the impact energy due to the much higher local velocity of a blade than a projectile, while the drone's velocity is related to the impact duration. The working conditions with low flight velocity and high rotating speed should be extensively concerned.
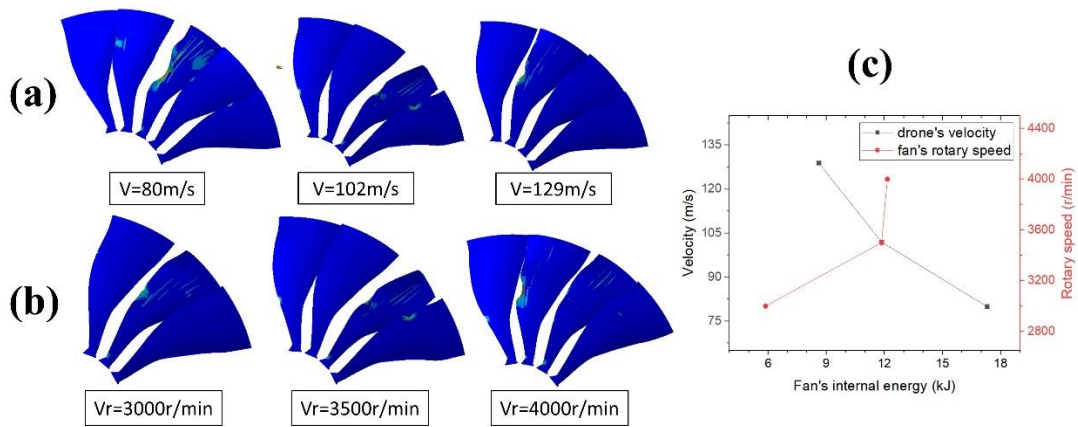

Figure 13 – Contour plots of the equivalent plastic strain of the fan blades shortly after the UAV collision with different values of (a) UAV's velocity and (b) fan's rotating speed, and (c) changing curves of the fan's internal energy with the variation of the drone's velocity and fan's rotating speed.

3.5 Comparison with bird strike

Fig.14(a) illustrates the colliding scenarios of both the UAV and bird impact cases with the same initial conditions. The deformation and failure of the fan blades are compared in Fig.14(b), which depicts the contour plots of the equivalent plastic strain of all affected blades. The numbers adjacent to blades represent their impacted sequence. It can be seen that the UAV strikes four fan blades while the bird impacts three due to the UAV's larger characteristic length (0.38m for UAV versus 0.207m for bird). Though the two projectiles share the same kinetic energy, the damage characteristics are quite different and analyzed as follows.

For a UAV collision, most of the UAV components bounces off after interacted with a blade, which exerts more concentrated force and results in fractures of the leading edge or pits on the surface. As is revealed in the top picture of Fig.14(b), Blade 1 and Blade 4 are both dented at their leading edges due to the impact of a motor, and further material failure occurred on Blade 4. A bird-strike event, however, performs a softer impact that the contact area promptly increases with the bird splashing, contributing to the reduction of local stress concentration. It is evidently observed in the bottom picture of Fig.14(b) that there is no material failure in any fan blades, though more intense plastic deformation is presented than the UAV case. Additionally, Blade 3 is subjected to the most intense plastic deformation in the UAV case while it is Blade 2 for the bird case. Both of them show certain torsion and bending patterns and their back surfaces also present a corrugated-shaped plastic deformation due to compressive stress. There is little plastic deformation observed on Blade 2 in the UAV case and Blade 3 in the bird case.
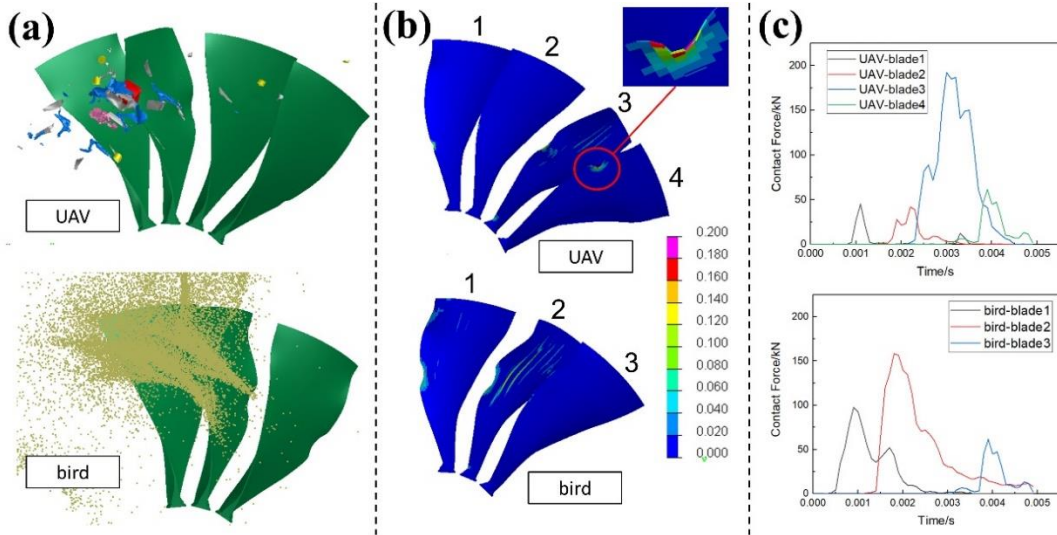
Figure 14 – (a) Colliding scenarios of the UAV and bird impact cases with the same impact energy, (b) contour plot of the equivalent plastic strain of the fan blades shortly after the UAV and bird collision, and (c) changing curves of the contact force of each affected blade induced by the UAV and bird impact.

Some clues can be found in Fig.14(c) to explain the different damage mechanics of the UAV and bird impact. One reason is the distinct material of the two projectiles. Most of the UAV constituents are made of metals and polymers, with the similar modulus and strength of the blades made of TC4. Therefore, the UAV-blade collision features hard impact and shows a higher peak force with a shorter duration (about 193kN with 2.5ms for the curve of UAV-blade3 in Fig.14(c)). On the contrary, the strength of the bird material is at least two orders of magnitude lower than that of the fan blade. Instead of the debris bouncing off from the blade in UAV case, the bird spreads and flows along the blade surface like a fluid, which presents a lower peak force with a longer duration (about 158kN with over 4ms for the curve of bird-blade2 in Fig.14(c)). Another reason is the different mass distribution. Though the UAV has the same total mass as the bird, the components with different weights are distributed non-uniformly as a result of its irregular geometric structure. The heaviest parts including the battery and the camera are mainly concentrated at the center of the UAV, and therefore more likely to be sliced by the same blade when confronted with a family of fan blades. Among all the contact force curves in the top graph of Fig.14(c), the maximum peak force is over four times larger than the others as a result of the highly-uneven weights of the different slices. As for the bird, however, it can be simplified to be homogeneous after neglecting its real interior tissues. Hence the fan blades cut the bird body into relatively-even partitions, which mitigate the contact force exerted on the individual blades. It is verified in the bottom graph of Fig.14(c) that the ratio of the maximum to second largest peak force reduces to around two.

There are some other significant parameters listed in Table 3 for quantitative comparison of the UAV and bird impact. Among all the factors, fan's internal energy and the maximum stress of the blade root represent the integral plastic deformation, while the maximum equivalent strain stands for the local damage of the blades. According to the results in Table 3, though the bird strike provokes a slightly higher level of the overall plastic deformation of the blades, the local damage and failure of blades caused by UAV collision are clearly more serious.

TABLE 3. Comparison of the UAV and bird impact

	UAV	Bird
Fan's internal energy (kJ)	11.849	13.179
Number of impacted blades	4	3
Occurrence of material failure of blades	YES	NO
Maximum equivalent plastic strain	0.2	0.146
Maximum Von-mises stress of the blade root (MPa)	1217.9	1227.8

Generally speaking, the damage and failure of the fan blades induced by UAV collision is more intense

than that by bird strike, accounting for the following reasons. One is that material failure of blades impacted by UAV may results in metal fragments. On the other hand, the rotating fan blades accelerate a cluster of UAV debris with far tougher materials than that of bird slices. Both incentives pose a threat to the casing containment, leading to the increased probability of catastrophic consequences.

4. Conclusions

In this paper, the dynamic response of a typical turbofan engine fan under UAV airborne collision is investigated by means of numerical simulation. The finite element models of the full-scale fan assembly and a typical small consumer quadcopter are established based on PAM-CRASH explicit analysis platform. A comparative study is also conducted between the bird and UAV ingestion with the same impact energy. The plastic deformation and failure of the fan blades are evaluated under different collision scenarios, with some conclusions shown as follows.

(1) The collision process between UAV and a single blade can be divided into two typical stages, slicing and impacting. When a drone is ingested into a rotating aeroengine fan, multiple blades will be affected, cutting the drone body into different weights of partitions which then induce various levels of deformation and failure in impacted blades. The majority of the fan's kinetic energy loss is transmitted to the drone's kinetic energy, accelerating its components at different levels, and the fan's internal energy, causing the deformation and damage of blades. The representative damage patterns of the fan blade include the overall torsion and bending deformation, and the dents or material failure at the leading edge.

(2) Results of the parameter study show that the impact orientation, the impact location and the impact energy all have significant effects on the fan's plastic deformation and failure. The most hazardous consequences occur when the drone with the yaw angle 0° and the pitch angle 45° collides the fan at 80° circular position. The closer the drone is to the blade tip, the larger the impact velocity will be, thus causing a higher damage severity in the fan blades. The drone poses an increasing threat on the fan blades with the drone's velocity decreasing or the fan's rotational speed increasing.

(3) Though the bird strike provokes a slightly higher magnitude of the overall plastic deformation of the blades, the local damage and failure of blades caused by UAV collision are clearly more serious. Different damage patterns and mechanics of the two projectiles are attributed to the distinct materials and mass distribution of their constituents. In summary, the damage and failure of the fan blades induced by UAV collision is more intense than that by bird strike due to its features of local stress concentration and material failure.

Contact Author Email Address

Yulong Li: liyulong@nwpu.edu.cn

Copyright Statement

References

[1] FAA, Federal Aviation Regulations/Aeronautical Information Manual (FAR/AIM) 2015: Bird ingestion certification standards, A.C. No. 33.76, Washington D.C.: Federal Aviation Administration (FAA), 2009.

[2] Song, Y., Horton, B., and Bayandor, J., "Investigation of UAS Ingestion into High-Bypass Engines, Part I: Bird vs. Drone," 58th AIAA/ASCE/AHS/ASC Structures, Structural Dynamics, and Materials Conference, Reston, Virginia: American Institute of Aeronautics and Astronautics, 2017.

[3] FAA Advisory Circular AC 107-2, "Small Unmanned Aircraft System (sUAS)", Washington, DC, 2016.

[4] D'Souza, K., Gregory, J.W., "Volume IV – UAS Airborne Collision Severity Evaluation–Engine Ingestion", Federal Aviation Administration, Draft Report, 2017.

[5] Xianghai Chai, Xiaoyun Zhang, Zhiqiang Wang and Yesheng Liu. Modeling of the Diffusion Bond for SPF/DB Titanium Hollow Structures, International Journal of Aerospace Engineering, Vol. 2015, No. 694564, 2015.

[6] Hou, Naidan; Li, Yulong; Liu, Jun, Numerical Simulation of Bird Impact on Hollow Blades of Titanium Fan Assembly, Journal of Aerospace Engineering, Vol.32, No.4, 04019044, 2019.

[7] Johnson, G. R., and W. H. Cook. Fracture characteristics of three metals subjected to various strains, strain rates, temperatures and pressures. Eng. Fract. Mech, Vol. 21, No. 1, pp 31–48, 1985. https://doi.org/10.1016/0013-7944(85)90052-9.

[8] Huang, J., Y. Z. Guo, D. Y. Qin, Z. X. Zhou, D. D. Li, and Y. L. Li. Influence of stress triaxiality on the failure behavior of Ti-6Al-4V alloy under a broad range of strain rates. Theor. Appl. Fract. Mech, Vol. 97, pp 48–61, 2018. https://doi.org/10.1016/j.tafmec.2018.07.008

[9] Meng Xianghao, Sun Yingjun, Yu Jingyu et al. Dynamic response of the horizontal stabilizer during UAS airborne collision. International Journal of Impact Engineering, Vol.126, pp 50–61, 2019.

[10] Sahraei E, Hill R, Wierzbicki T. Calibration and finite element simulation of pouch lithium-ion batteries for mechanical integrity. J Power Sources, Vol.201, No.3, pp.307–21, 2012.

[11] Meguid SA, Mao RH, Ng TY. FE analysis of geometry effects of an artificial bird striking an aeroengine fan blade. Int J Impact Eng., Vol.35, No.6, pp.487–98, 2008.

[12] Vignjevic, R., M. Orlowski, T. D. Vuyst, and J. C. Campbell. A parametric study of bird strike on engine blades." Int. J. Impact Eng., Vol.60, pp.44–57. 2013. https://doi.org/10.1016/j.ijimpeng.2013.04.003.

[13] Lavoie, M. A., A. Gakwaya, M. N. Ensan, D. G. Zimcik, and D. Nandlall. Bird's substitute tests results and evaluation of available numerical methods. Int. J. Impact Eng., Vol. 36, No.10–11, pp.1276–1287, 2009. https://doi.org/10.1016/j.ijimpeng.2009.03.009.

[14] Lucy, L. B. A numerical approach to testing the fission hypothesis. Astron. J., Vol.82, No.12, pp.1013–1024, 1977. https://doi.org/10.1086/112164.

[15] Liu, J., Y. L. Li, and X. H. Gao. Bird strike on a flat plate: Experiments and numerical simulations. Int. J. Impact Eng., Vol.70, pp.21–37, 2014. https://doi.org/10.1016/j.ijimpeng.2014.03.006.

[16] McCarthy MA, Xiao JR, McCarthy CT, et al. Modelling bird impacts on an aircraft wing Part 2: modelling the impact with an SPH bird model. Applied Composite Materials, Vol.11, No. 5, pp. 317-340, 2004.